Journal of Biomedical Optics 8(3), 396–409 (July 2003)

Multiphoton microscopy: an optical approach to understanding and resolving sulfur mustard lesions*

Robert J. Werrlein
Janna S. Madren-Whalley
U.S. Army Medical Research
Institute of Chemical Defense
Aberdeen Proving Ground, Maryland 21010-5400
E-mail: Robert.Werrlein@amedd.army.mil

Abstract. Sulfur mustard (SM; 2,2′-dichloroethyl sulfide) is a percutaneous alkylating agent first used as a chemical weapon at Ypres, Belgium, in World War I. Despite its well-documented history, the primary lesions effecting dermal–epidermal separation and latent onset of incapacitating blisters remain poorly understood. By immunofluorescent imaging of human epidermal keratinocytes (HEK) and epidermal tissues exposed to SM (400 μM for 5 min), we have amassed unequivocal evidence that SM disrupts adhesion complex molecules, which are also disrupted by epidermolysis bullosa-type blistering diseases of the skin. Images of keratin 14 (K14) in control cells showed tentlike filament networks linking the HEK's basolateral anchoring sites to the dorsal surface of its nuclei. Images from 6-h postexposure profiles revealed early disruption ($\leqslant$1 h) and progressive collapse of the K14 cytoskeleton. Collapse involved focal erosions, loss of functional asymmetry, and displacement of nuclei beneath a mat of jumbled filaments. In complementary studies, 1-h images showed statistically significant ($p<0.01$) decreases of 25 to 30% in emissions from labeled $\alpha_6\beta_4$ integrin and laminin 5, plus disruption of their receptor–ligand organization. Results indicate that SM alkylation destabilizes dermal–epidermal attachments and potentiates vesication by disrupting adhesion complex molecules and associated signaling mechanisms required for their maintenance and repair. [DOI: 10.1117/1.1584687]

Keywords: multiphoton microscopy; human epidermis; adhesion complex; keratinocytes; sulfur mustard; keratin 14 cytoskeleton; $\alpha_6\beta_4$ integrin; laminin 5.

Paper MM-04 received Oct. 15, 2002; revised manuscript received Dec. 11, 2002; accepted for publication Dec. 23, 2002.

1 Introduction

Multiphoton microscopy[1–3] and high-resolution imaging of human epidermal tissues and keratinocytes (HEK) are providing detailed information about the molecular injuries and pathogenic manifestations produced by exposure to sulfur mustard (SM). Sulfur mustard is a lipophilic, percutaneous, alkylating agent that readily penetrates the stratum corneum and produces prevesicating lesions within 2 min of exposure.[4] This agent has been used by warring nations for more than 80 years, and the global prospect of exposure to SM is probably greater today than at any time since World War I. Still, there is no completely effective treatment against its toxicity. Efforts to develop mechanistically based treatment strategies are confounded by not knowing precisely how the inherent characteristics of skin are altered so that the epidermal–dermal junction becomes the specific site for blister formation. We know from other work that mutations causing altered assembly or absence of epidermal keratins can produce blistering diseases of the skin.[5–10] We also know from our own studies[11–12] that keratins K5 and K14 are early SM targets. In that regard, epidermolysis bullosa simplex (EBS, a family of blistering skin diseases) has generally been associated with mutations and abnormal assembly of these same heterodimeric keratins.[13–14]

However, EBS blisters occur above the hemidesmosomes[14] and not at the epidermal–dermal junction, as do SM blisters.[15,16] Accordingly, we have tried to determine whether the toxic effects of SM on keratin filaments also include associated proteins and ultimately the structural integrity of adhesion complex molecules. The rationale for that question lies in knowing that hemidesmosomes link transmembrane $\alpha_6\beta_4$ integrin receptors to keratin filaments[17] and to the basement membrane via plectin,[18–21] bullous pemphigoid antigens,[14,22,23] and laminin 5.[24,25] Mutations that disrupt the assembly of $\alpha_6\beta_4$ integrin or laminin 5 are causative factors in junctional epidermolysis bullosa (JEB), another family of blistering skin diseases.[26] Based on similarities between SM- and JEB-induced vesication, we have postulated that the blisters produced by sulfur mustard may share a similar pathology, i.e., may result from disruptions in the subcellular assembly of adhesion complex molecules. Multiphoton microscopy is providing us with the spatial resolution to test this hypothesis.

*A preliminary report of this work appeared in *Proc. SPIE* **4620**, 231–234 (2002).

1083-3668/2003/$15.00

2 Materials and Methods

2.1 *Human Epidermal Keratinocyte Cultures*

Human epidermal keratinocyte cultures (Clonetics/Cambrex, Walkersville, Maryland) were grown on borosilicate glass coverslips in Clonetics' keratinocyte growth medium (KGM) at 37 °C in a humidified atmosphere of 5% CO_2 in air. Replicate cultures were maintained in exponential growth to densities of ~50,000 cells/cm^2, i.e., until they were approximately 70% confluent, and were subjected to renewal of the medium 2 h prior to SM exposure.

2.2 *Human Epidermal Tissues*

Tissues were prepared as previously described[27] by gentle proteolytic treatment of surgical explants obtained from the Cooperative Human Tissue Network (Ohio State University, Columbus, Ohio). Intact tissue preparations were maintained at 6 °C in KGM and then warmed to room temperature immediately prior to SM exposure.

2.3 *Sulfur Mustard Exposures*

Sulfur mustard exposures were the same for HEK cultures and epidermal tissues. Supernatant media were removed from replicate culture and tissue dishes and were replaced with prewarmed (37 °C) KGM for sham-treated controls or with prewarmed KGM containing 400 μM SM. After a 5-min exposure, all cultures and tissues were washed three times with fresh KGM and returned to the CO_2 incubator.

2.4 *Postexposure Fixing and Immunofluorescent Staining of HEK and Epidermal Tissues*

The HEK cultures were fixed with 4% paraformaldehyde for 10 min at room temperature for the study of α_6 integrin and laminin 5, and were postfixed (permeabilized) for 3 min with 100% acetone at −20 °C for the study of keratin 14. Epidermal tissues were fixed overnight at 6 °C with modified Karnovsky's fixative consisting of 2.5% glutaraldehyde and 1.6% paraformaldehyde in 0.1 M sodium cacodylate, pH 7.4. Using indirect staining, the HEK and epidermis were incubated 1 h at room temperature with one of the following primary antibodies diluted in phosphate buffered saline (PBS). A 1:200 dilution of mouse antihuman keratin 14, clone LL002 (Neo Markers Inc., Fremont, California); a 1:50 dilution of mouse antihuman α_6 integrin (Harlan, Sera-Lab Ltd., Loughborough, England); a 1:50 dilution of mouse antihuman laminin 5 γ2 chain (Chemicon International, Temecula, California). For dual labeling of α_6 integrin and laminin 5, we used a 1:50 dilution of rat antihuman α_6 integrin (Chemicon). Cells and tissues were then washed (three times, 3 min each) and incubated 1 h in the dark with the appropriate secondary antibody (as indicated). For single labels, we used a 1:50 dilution of fluorescein isothiocyanate (FITC)-conjugated goat antimouse immunoglobulin G (IgG; heavy and light chain H & L) (Accurate Chemical and Scientific Corp., Westbury, New York). For dual labels, we used a 1:200 dilution of Alexa488-conjugated goat antimouse IgG (H & L) and Alexa568-conjugated goat antirat IgG (H & L) (Molecular Probes Inc., Eugene, Oregon).

2.5 *Counterstaining Cells with Propidium Iodide*

When counterstaining nuclei with propidium iodide (PI; Molecular Probes Inc.), attached HEK (already processed for K14) were equilibrated in 2× (SCC) (0.3 M NaCl, 0.03 M sodium citrate; pH 7.0), incubated for 20 min at 37 °C with 100 μg/ml ribonuclease (RNAse) IIA (Sigma Chemical Co., St. Louis, Missouri), then washed and stained for 5 min with PI (32 μM) and washed again in PBS prior to imaging as wet mounts.

2.6 *Multiphoton Imaging*

Imaging was performed with an MRC-1024 multiphoton laser-scanning system (Bio-Rad, Hemel Hempstead, United Kingdom) using an Axiovert-135 inverted microscope and a C-Apochromat 63×/1.2 NA water objective (Carl Zeiss Inc., Thornwood, New York). Excitation was conducted at 780 nm using a Verdi 5-W diode pump and a Mira 900 Ti:sapphire pulsed laser with X-wave optics (Coherent Laser Group, Santa Clara, California). Fluorescent emissions were directed through an E625 short-pass (SP) filter, an HQ 575/150 filter and then onto external detectors. For cell and tissue preparations labeled with a single fluorochrome, emissions were detected at photomultiplier tube-1 (PMT-1) without additional filtering. For dual imaging of preparations labeled with two fluorochromes, the coincident red and green emissions were split by a 550 dichroic long-pass (DCLP) filter, which allowed red light to pass through a D630/60 bandpass filter to PMT-1 and reflected green emissions through a D525/50 filter to PMT-2. These filters (Chroma Technology Corp., Brattleboro, Vermont) allowed resolution of target molecules without bleedthrough between detectors.

2.7 *Analyses of the Images*

Analyses were performed using a combination of Bio-Rad's LaserSharp software, complementary Meridian software, and Microsoft Excel. The average results for control and exposed populations are presented as the mean ±SEM. Student's *t*-test was used for statistical comparison with probabilities of $p < 0.01$ regarded as statistically significant.

3 Results

3.1 *Collapse of the Keratin 14 Cytoskeleton*

Immunofluorescent images from replicate HEK cultures showed that keratin 14 filaments and their intracellular organization are exquisitely sensitive to SM alkylation. In 6-h postexposure profile studies, high-resolution stereo images (Figs. 1 and 2) showed that vesicating doses of sulfur mustard caused early disruption and progressive collapse of the K14 cytoskeleton. Cells in control populations maintained a characteristic airy, interlacing network of filaments [Figs. 1(a), 1(c), and 2(a)]. Each cell, regardless of shape, had a tentlike organization of K14 filaments that extended out and down from the dorsal surface of the raised central nucleus to a narrow rim of basolateral anchoring sites. The presence of numerous epithelial shapes in subconfluent, control populations was an expression of functional asymmetry, i.e., basal cell capacity to reorganize and configure its K14 filament arrangements to meet the dynamics of polarized mobility.

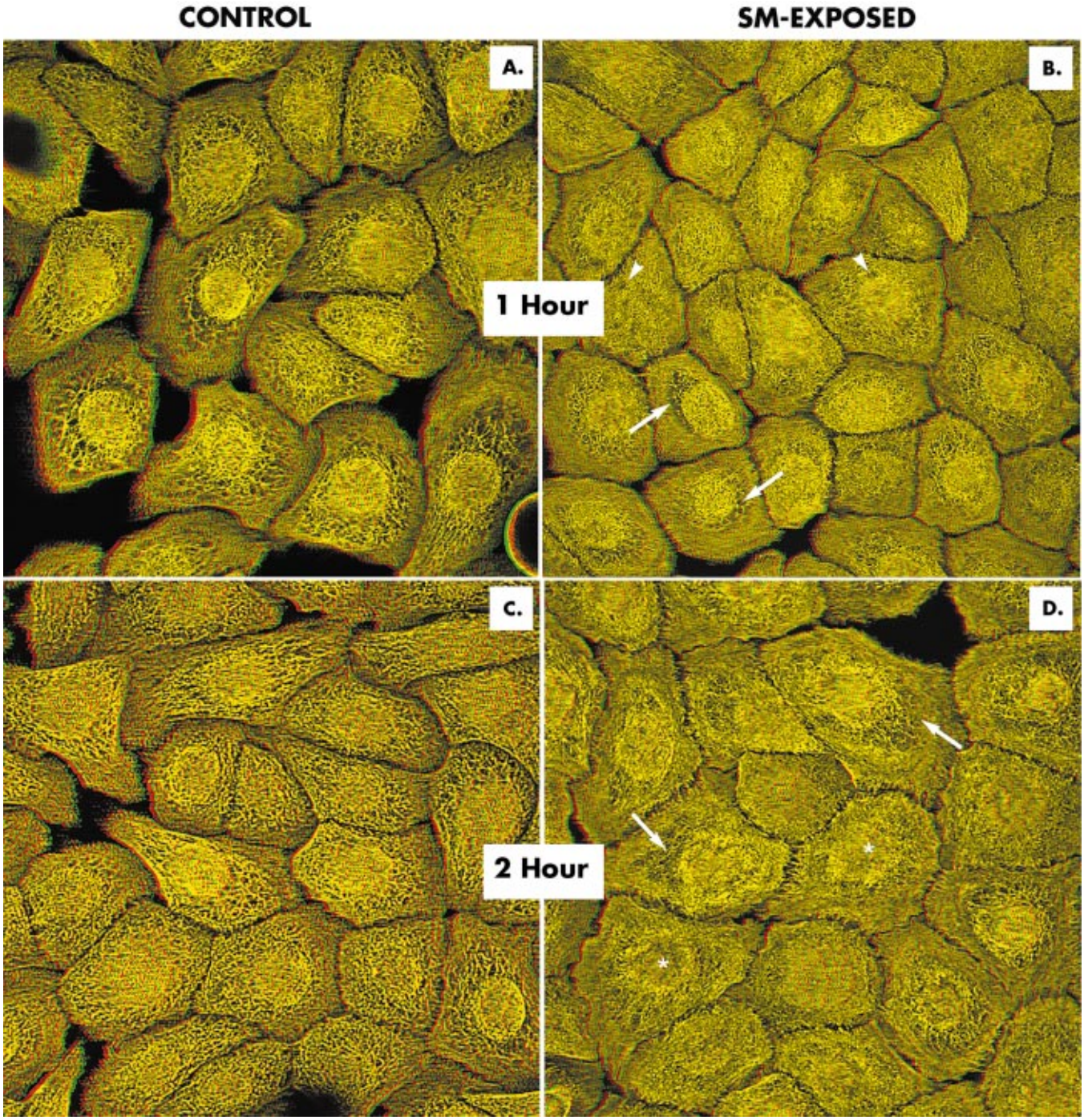

Fig. 1 Effects of SM on the keratin 14 cytoskeleton. (To view with 3-D glasses, place green lens over right eye; for inverted view place red over right eye.) Images from HEK control populations (a) and (c) show that K14 filaments of subconfluent cells are organized into interlacing, tentlike, airy networks. Each network envelops the dorsal surface of its raised central nucleus and extends down to a narrow rim of basolateral anchoring sites (inverted view). The presence of numerous epithelial shapes reveals the polarized mobility and functional asymmetry of these cells. At 1 h after exposure (b), there was an obvious reduction in the open, airy appearance of K14 networks. There were early indications of focal erosion (arrowheads), retraction of basolateral filaments, cell–cell separations, and partial collapse of the cytoskeleton, resulting in stretching of filaments over the nuclei (arrows). At 2 h after exposure (d), the images showed substantial disruption in the organization of K14 filaments, progressive collapse of the cytoskeleton (inverted view), nuclear displacement to the cell's attachment surface (asterisk), perinuclear stretching of filaments (arrows), and loss of functional asymmetry (i.e., polarized mobility).

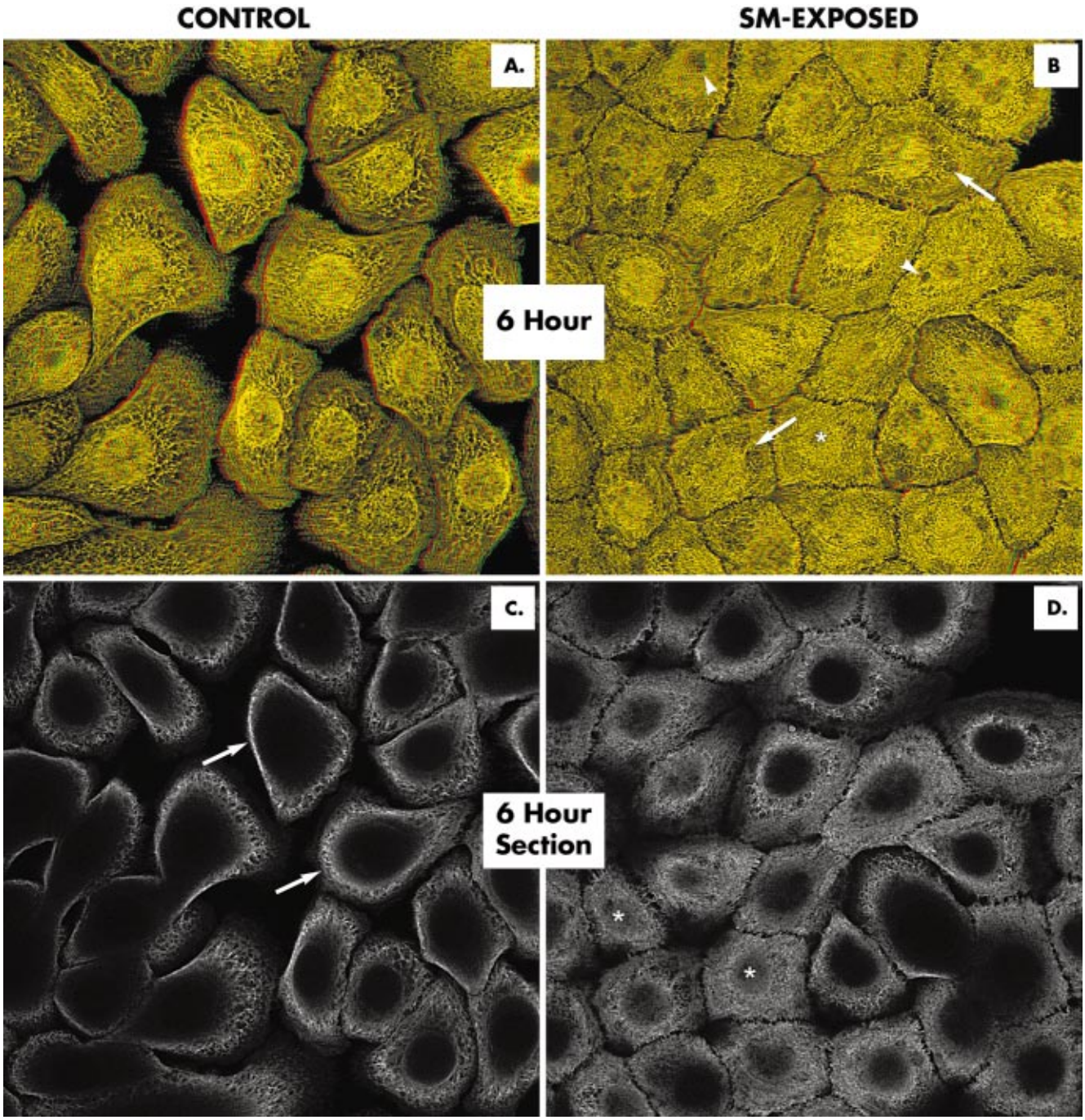

Fig. 2 Effects of SM on the keratin 14 cytoskeleton. At 6 h postexposure, control cells (a) maintained their characteristic, airy, tentlike organization of K14 filaments and their functional asymmetry. Exposed cells (b) had numerous focal erosions (arrowheads) and severely displaced nuclei (asterisk) beneath the jumbled mat of collapsed and stretched filaments (arrows). The prevalence of geometric cell shapes indicated a persistent loss of functional asymmetry and polarized mobility. A comparison with serial 0.5-μm sections taken at 2.0 μm from the HEK attachment surface showed peripheral, airy bands of keratin filaments (arrows) in cells from the control population (c). These K14 bands were circumscribed around relatively large, nonfluorescent intracellular areas containing no keratin filaments. Sections from the SM-exposed population (d) showed extensive perinuclear mats of collapsed filaments that filled the intracellular space and occasionally covered the displaced nuclei (asterisks).

At 1 h after exposure, the images showed substantial reductions in the open, airy appearance of K14 networks [Fig. 1(b)]. These images revealed early signs of focal erosion in the K14 cytoskeleton, retraction of basolateral filaments, intercellular separations, and partial collapse (with stretching) of filaments over the raised, central nuclei.

At 2 h after exposure, the images showed severe progressive collapse of the K14 cytoskeleton [Fig. 1(d)], with almost complete disruption of its open, latticelike organization. Progressive collapse over the nuclei exacerbated perinuclear stretching of filaments and caused nuclear displacement to the HEK attachment surface. The images also indicated progressive loss of functional asymmetry, i.e., polarized mobility.

At 6 h after exposure, there were numerous focal erosions [Fig. 2(b)] and severe nuclear displacements beneath the jumbled mats of collapsing filaments. Loss of HEK mobility persisted and was characterized by retraction of basolateral filaments, intercellular separations, loss of functional asymmetry, and accumulation of more regular, geometric cell shapes.

From the 6-h control and SM-exposed populations [Figs. 2(a) and 2(b)], serial sections taken at increments of 0.5 μm from the attachment surface gave further evidence for the extensive collapse of the K14 cytoskeleton. Control images at 2 μm from the attachment surface [Fig. 2(c)] showed narrow peripheral bands of open, airy, keratin filaments circumscribed around a relatively large, nonfluorescent intracellular area containing no K14 filaments. Images from the 2-μm section of the SM-exposed population [Fig. 2(d)] showed broad perinuclear mats of collapsed filaments that filled the intracellular space and occasionally covered the severely displaced nuclei. Western blots and densitometry studies (not shown) confirmed that there was no postexposure increase in K14 concentration (Dillman et al., unpublished data).[28]

With multiphoton excitation and dual emission techniques, images from 2-h control populations [Fig. 3(a)] showed that FITC-labeled K14 filaments (λ_{em} 518 nm) co-localized on the uppermost surface of propidium-iodide labeled nuclei (λ_{em} 617 nm). Co-localization revealed an orange, gridlike pattern of filament-to-nucleus attachments. In exposed populations, cytoskeletal collapse obscured the orange color and detail of filament attachments [Fig. 3(b)]. The extent of collapse and its potential for adversely affecting signal transduction became more evident when optical slices were compared. Images taken at 3.5 μm from the HEK attachment surface showed control populations with peripheral rings of K14 filaments set well apart from the main body of each nucleus [Fig. 3(c)]. At 2 h postexposure, images taken at 3.5 μm from the attachment surface showed that the intracellular space and nuclei of most HEK were awash in a mat of collapsed filaments [Fig. 3(d)]. Typically, there was an accumulation of geometric cell shapes in each image field, indicating an SM-induced loss of mobility and functional asymmetry.

Collapse of the K14 cytoskeleton, as illustrated in Fig. 4 revealed that SM alkylation disrupted the dynamic organization of filaments linking each nucleus to its plasma membrane. That effect almost certainly disrupts normal signaling between these elements. Since $\alpha_6\beta_4$ integrins are uniquely adapted for linking K14 to the HEK attachment surface,[17,18,21] the following studies were undertaken to enhance our understanding of SM effects on both cell adhesion and the structures affecting signal transduction.

3.2 *Imaging of $\alpha_6\beta_4$ Integrin and Laminin 5 in HEK Cultures*

Dual imaging of $\alpha_6\beta_4$ integrin and laminin 5 (Fig. 5) located the brightest emissions from these molecules at the basolateral membrane margins of the constituent HEK. Overall distribution of these molecules relative to keratin 14 was determined by viewing (0.5-μm) serial sections from 3-D reconstructions starting at the level of cell-to-substrate attachment and moving up through as many as 25 Z-series slices [Fig. 5(a)]. Alexa dyes 568 and 488 conjugated to $\alpha_6\beta_4$ integrin and laminin 5, respectively, showed that a majority of the integrins [Fig. 5(b)] and all of laminin 5 [Fig. 5(c)] were contained in the first two sections, i.e., within 0.5 μm of the attachment surface. Dual imaging of these molecules confirmed that in subconfluent, mobile populations, $\alpha_6\beta_4$ integrin was co-localized on extracellular laminin 5 tracks. The integrins appeared as well-defined, narrow (orange) bands at the basolateral membrane margins of HEK [Fig. 5(d)], which also contains anchoring sites for the K5/K14 cytoskeleton.

In control populations stained for α_6 integrin, the membrane margins of mobile cells frequently expressed brightly fluorescent filopodial-type retraction fibers [Fig. 6(a)]. At 1 h after exposure, however, there was a statistically significant ($p<0.01$) 27% decrease in fluorescence intensity, an obvious reduction in retraction fibers, and a concomitant loss of functional asymmetry [Fig. 6(b)]. Similar results were previously reported for β_4 integrin.[11]

Postexposure studies of the laminin 5 ligand *in vitro* produced images that were complementary to those from $\alpha_6\beta_4$ integrin, its adhesion receptor. At 1 h after exposure, there was a statistically significant 32% decrease in the extracellular laminin 5 volume and a corresponding decrease in image intensity. Image outlines conformed to the basolateral shapes of the constituent HEK and affirmed the loss of polarized mobility (Fig. 7). It is worth noting that the *in vitro* image patterns from all three interactive molecules (keratin 14, $\alpha_6\beta_4$ integrin, and laminin 5) attest to a postexposure loss of mobility and functional asymmetry.

3.3 *Imaging of $\alpha_6\beta_4$ Integrins and Laminin 5 in Human Epidermis*

The structural organization and the response of $\alpha_6\beta_4$ integrins to sulfur mustard were particularly revealing in intact, epidermal tissues. In 3-D reconstructions, focal sites found on the membrane margins of basal cells appeared to define the origins and insertions of $\alpha_6\beta_4$-integrin subunits [Fig. 8(a)]. These sites gave rise to stalked exodomains that fused apically and produced relatively long, narrow, bridging strips that traversed the surface of one or more adjacent cells. Ultimately, these bridging strips coalesced to produce a complex, highly textured matrix of receptors that covered the entire ventral, basal cell surface with circular, porelike structures having an inner diameter of approximately 1 μm.

Production of laminin 5 by epidermal tissues was typically found only in isolated basal cell clusters [Fig. 9(a)], indicating

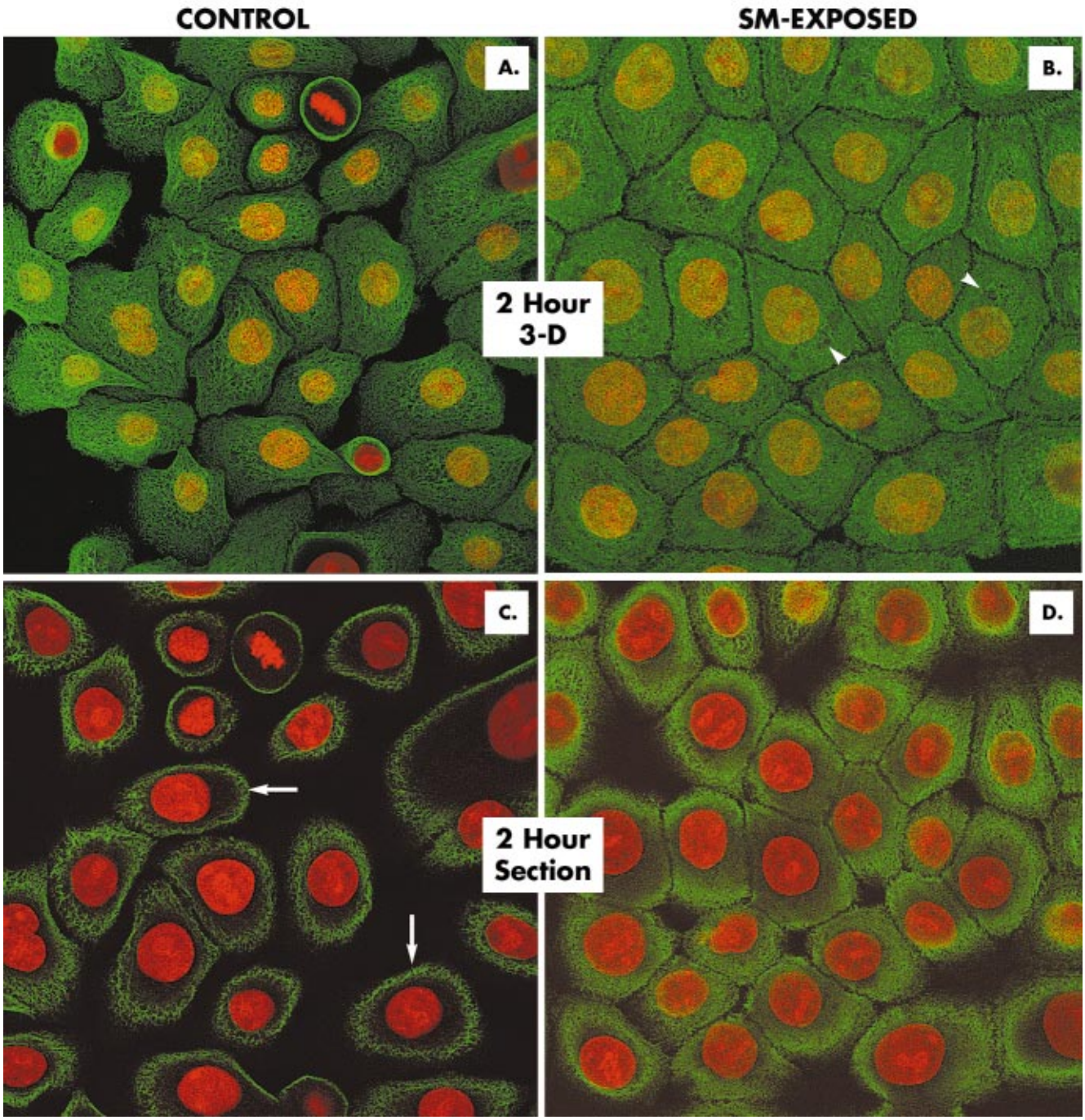

Fig. 3 Dual imaging of SM effects on K14 and the HEK nuclei. At 2 h postexposure, the control population (a) showed that green, FITC-tagged K14 filaments co-localized on the red, dorsal surface of propidium iodide-stained nuclei. Co-localization revealed an orange gridlike pattern of filament-to-nucleus attachments. The images of the numerous epithelial cell shapes also confirmed the functional asymmetry of these healthy, mobile cells. In an exposed population (b), collapsed filaments partially obscured the nucleus and its cytoskeletal attachments. Lesions included focal erosions (arrowheads) and loss of functional asymmetry. A comparison with 0.5-μm optical sections taken at 3.5 μm from the attachment surface showed that sections from each cell in the control population had a peripheral ring of K14 filaments (c, arrows), which was set well apart from the central nucleus. Sections from the exposed population (d) showed each nucleus awash in an amorphous mat of collapsed filaments.

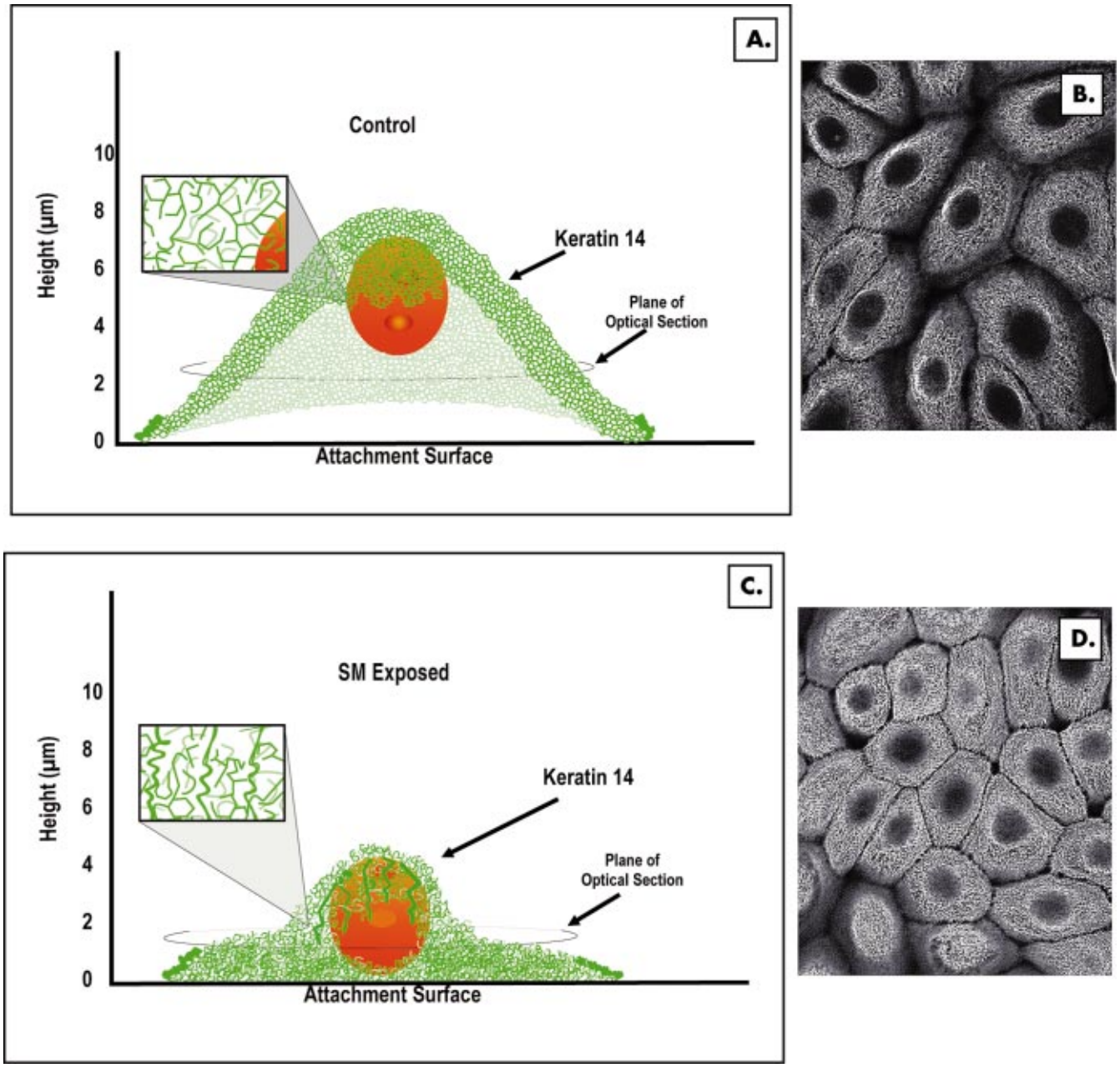

Fig. 4 Composite of SM effects on the K14 cytoskeleton and HEK nucleus. Control HEK (a) maintained a characteristic, tentlike organization of airy, interlacing keratin 14 filaments. Each active network produced focal, gridlike attachments to the dorsal surface of the raised, central nucleus (see exploded view). In 0.5-μm optical sections taken at 2 and 3.5 μm from the attachment surface of control HEK [Fig. 2(c) and Fig. 3(c)], the images showed peripheral rings of K14 filaments that made no direct contact with the central nucleus. In 3-D reconstructions containing additional cell sections, the images showed that K14 filaments do make direct contact with (and surround) the dorsal surface of HEK nuclei (b). In cells from exposed populations (c), progressive collapse of the K14 cytoskeleton displaced each nucleus to the HEK attachment surface. The displaced nuclei were found to be enveloped in a jumbled mat of collapsed filaments at and near the attachment surface (d).

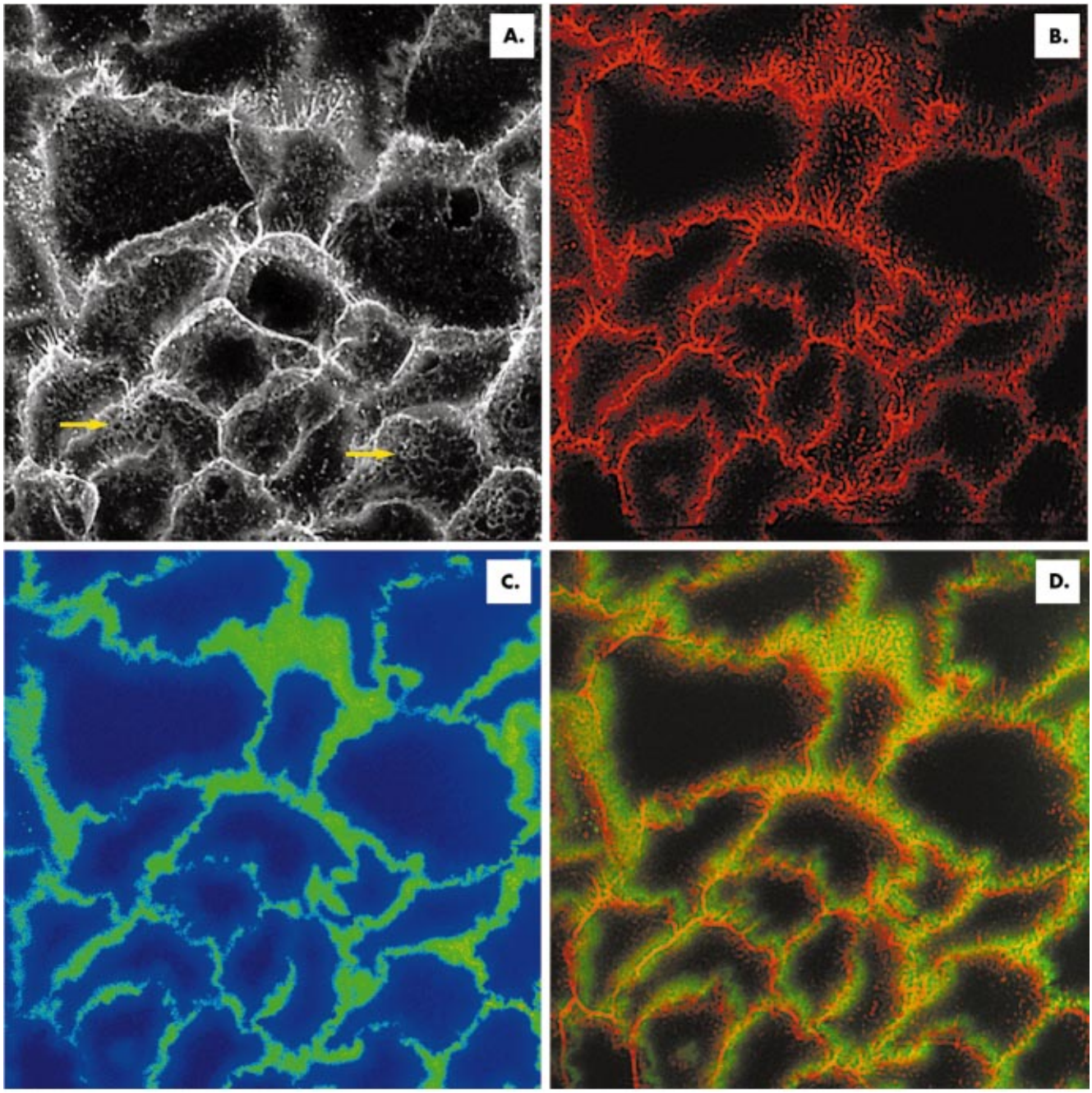

Fig. 5 Dual imaging of α_6 integrin and laminin 5 in an HEK culture. A 3-D reconstruction (a) displays both molecules in gray tone. It shows a faint veil or covering of α_6 integrins containing some circular α_6 integrin structures loosely organized and barely visible on the upper cell surface (arrows). Optical sections taken within 0.5 μm of the HEK attachment surface contained the large majority of $\alpha_6\beta_4$ integrins, seen as red emissions (b), and contained all of the green emissions from laminin 5(c). These two molecules co-localized at the HEK attachment surface and expressed an orange, basolateral image track wherever the $\alpha_6\beta_4$ integrin receptors attached to their laminin 5 ligand.

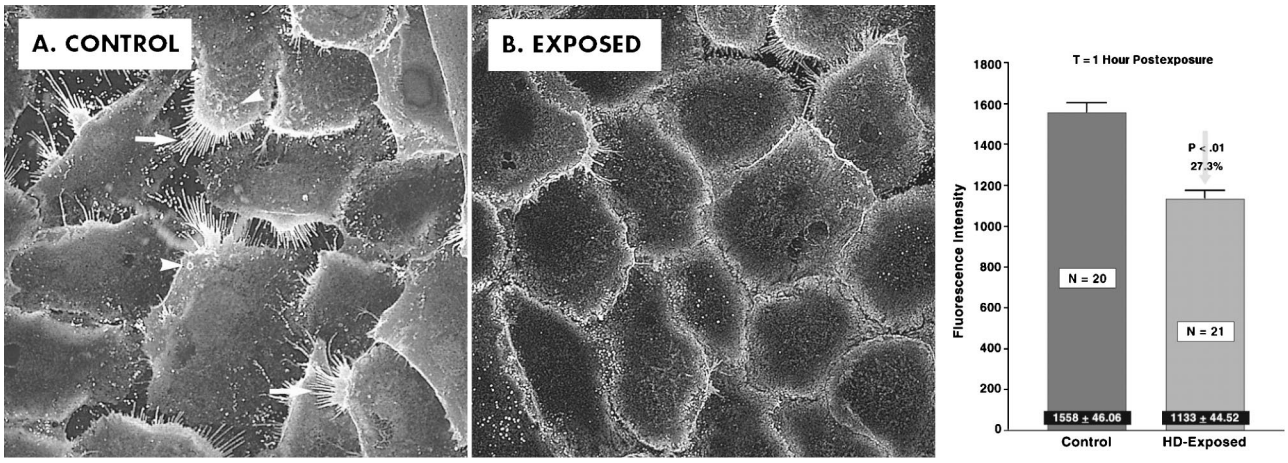

Fig. 6 Sulfur mustard effects on α_6 integrin in HEK cultures. A sham-treated control population (a) shows cells with a slightly textured surface of α_6 integrins, organized to include indistinct, circular, porelike structures (arrowheads). The emissions were brightest along the basolateral margins of cell attachment and in the trailing filopodial-like retraction fibers (arrows). At 1 h after exposure, there was a statistically significant ($p<0.01$) 27.3% decrease in image intensity. There were disruptions in the cell's α_6 integrin surface (b), including almost complete loss of retraction fibers and functional asymmetry, i.e., a striking change to less mobile, geometric cell shapes.

that *de novo* synthesis was discontinuous. During active laminin 5 production, images of the γ-2 chain precursor showed that the process included reduction, polarization, and movement of a single punctate, laminin 5 isoform to the ventral surface of each basal cell [Fig. 9(b)]. As a result, each punctate unit became attached to an anchoring site on the epidermal surface, forming a laminin 5 ligand cluster at the epidermal–dermal junction [Fig. 9(c)].

By dual imaging of α_6 integrin and laminin 5 in human epidermis (Fig. 10), the co-localization of punctate laminin 5 units [Fig. 10(b)] and circular α_6-integrin surface structures [Fig. 10(a)] was resolved. The images showed that the orange, laminin 5 anchoring sites were positioned on the outer rim of the circular $\alpha_6\beta_4$ surface receptors. It is interesting to note that solitary basal cells were occasionally engaged in laminin 5 synthesis and movement activity [Fig. 10(d)]. In such cases, delivery and precise placement of the ligand on a circular integrin anchoring site was conducted through elongated cytoplasmic extensions.

Following exposure to sulfur mustard, we observed severe disruption of the $\alpha_6\beta_4$ surface receptors. Within 1 h of exposure, there was unraveling of the circular, porelike structures and retraction of the extracellular assemblies to their origins and insertions on the plasma membrane margins [Fig. 8(b)]. The effect was characterized by an almost total loss in the organization and surface expression of $\alpha_6\beta_4$ integrins. Depletion of these adhesion receptors would obviously result in a concomitant loss of laminin 5 anchoring sites. That would in effect weaken the attachment complex. It should be noted, however, that disassembly and depletion of $\alpha_6\beta_4$ integrins also occurred spontaneously following dermal–epidermal

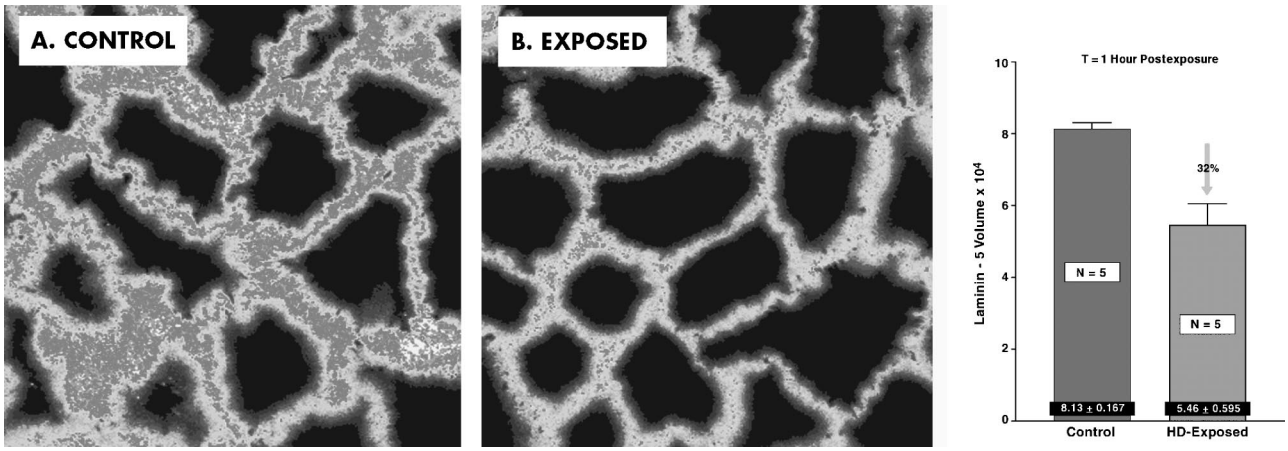

Fig. 7 Sulfur mustard effects on laminin 5 in HEK cultures. The 3-D reconstruction from the control population (a) shows a brightly fluorescent, ropy deposit of intercellular laminin 5. At 1 h postexposure, there was a decrease in image intensity (b), a statistically significant ($p<0.01$) 32% decrease in laminin 5 volume, and an altered pattern of intercellular laminin 5 that reflected associated changes in cell shape and loss of polarized mobility.

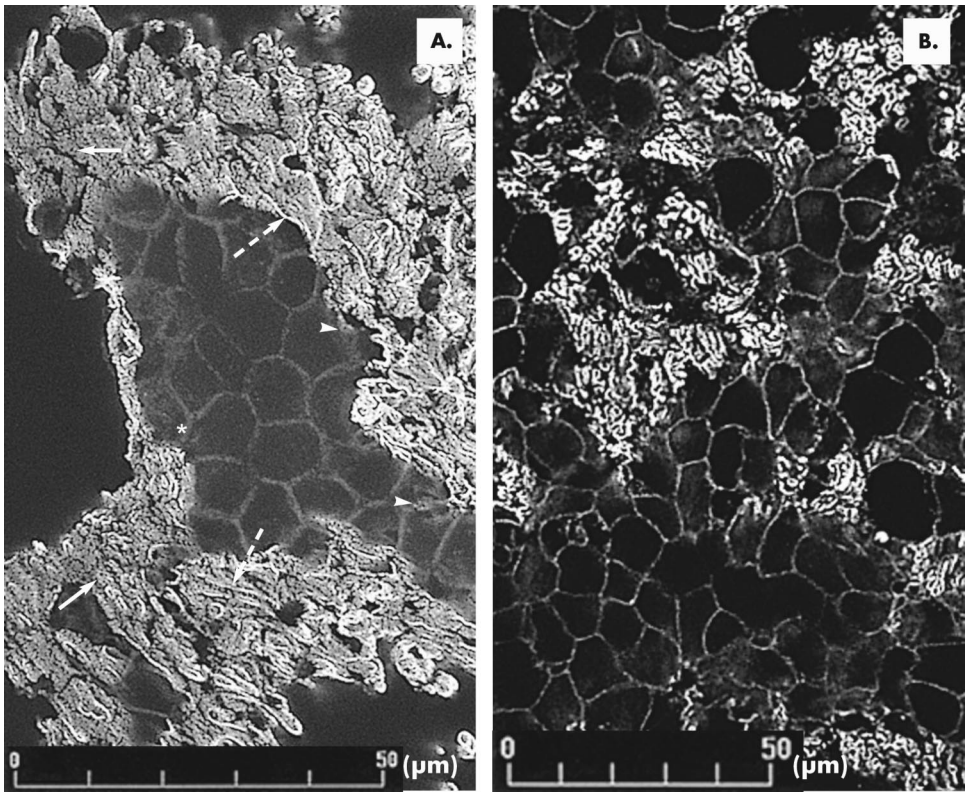

Fig. 8 Effect of SM on $\alpha_6\beta_4$ integrin organization. The 3-D reconstruction of α_6 integrin on a ventral surface of human epidermis (a) revealed focal sites on the basal cell's membrane margins (arrowheads) that located the origins and insertions (for the exodomains) of $\alpha_6\beta_4$ integrin receptors. Each site gave rise to a stalked α_6 integrin subunit. These stalked subunits coalesced apically to form bridging strips (dashed arrows) that traversed the surface of one or more cells. Within these bridging strips, the integrin subunits repeated at regularly spaced intervals of approximately 1 μm. Ultimately, the interconnected subunits became organized into a complex matrix that covered the entire basal cell surface with $\alpha_6\beta_4$ integrin strips and circular, porelike structures (solid arrows). At 1 h after SM exposure (b), the well-organized integrin exodomains were severely disrupted. The images showed unraveling of the strips and circular, porelike structures, and retraction of α_6 integrins from these surface assemblies to their origins and insertions on the plasma membrane margins. Identical results were obtained with the β_4 integrin subunit (data not shown).

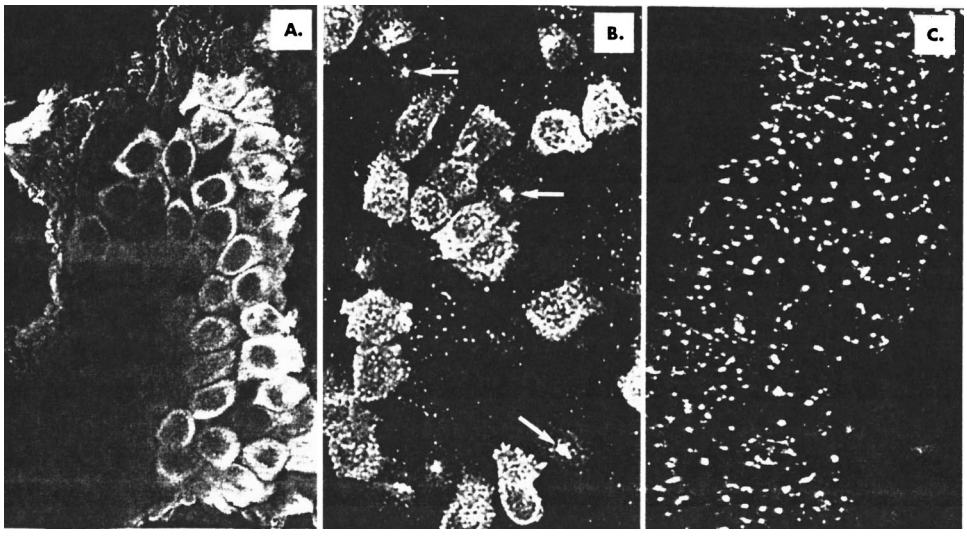

Fig. 9 Laminin 5 production in intact human epidermis was typically found only in scattered clusters of HEK within the stratum basale (a), indicating that *de novo* synthesis was discontinuous. Processing of laminin 5 involved reduction and polarization of the γ2-chain precursor and resulted in production of punctate laminin 5 isoforms (arrows, b). After moving to the ventral epidermis, the punctate isoforms became integrated into the basal cell's adhesion complex as attachment site clusters (c).

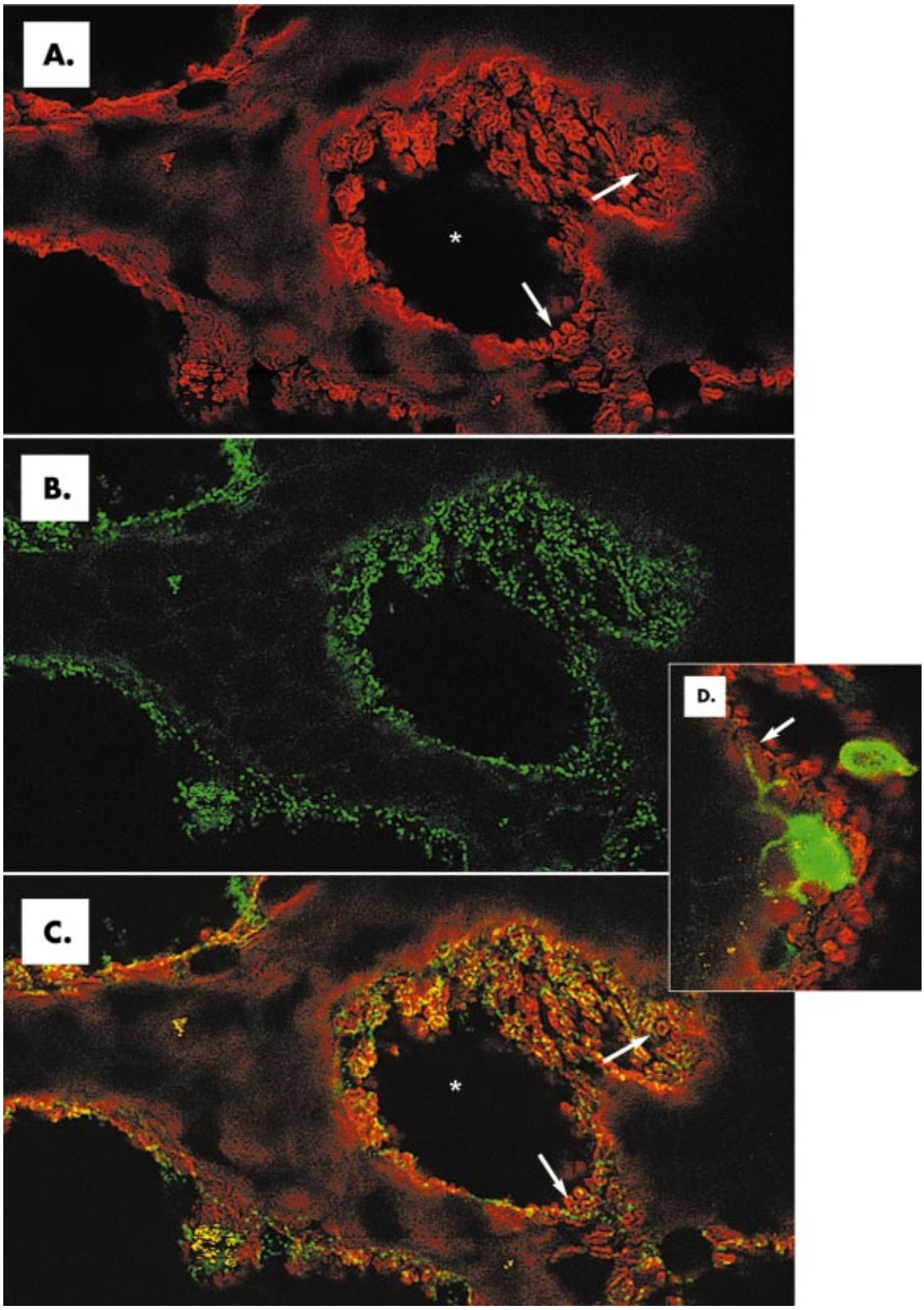

Fig. 10 Dual imaging of Alex568-conjugated α_6 integrin and Alexa488-conjugated laminin 5 in the human epidermis. A 3-D reconstruction (a) shows a red ventral epidermis with circular, α_6 integrin surface receptors (arrows) that collectively surround a nonfluorescent central cavity, i.e., dermal papillae (asterisk). In (b) the presence of a green, punctate, laminin 5 isoform is shown in the same epidermal image field. Dual imaging of both molecules revealed an orange co-localization of the punctate laminin 5 ligand on the outside rim of the circular α_6 integrin receptors (c, arrows). In isolated laminin 5-producing cells (d), we observed that movement was conducted via thin cytoplasmic extensions of the cell to the outer rim (anchoring site?) of circular α_6 integrin surface receptors (arrow).

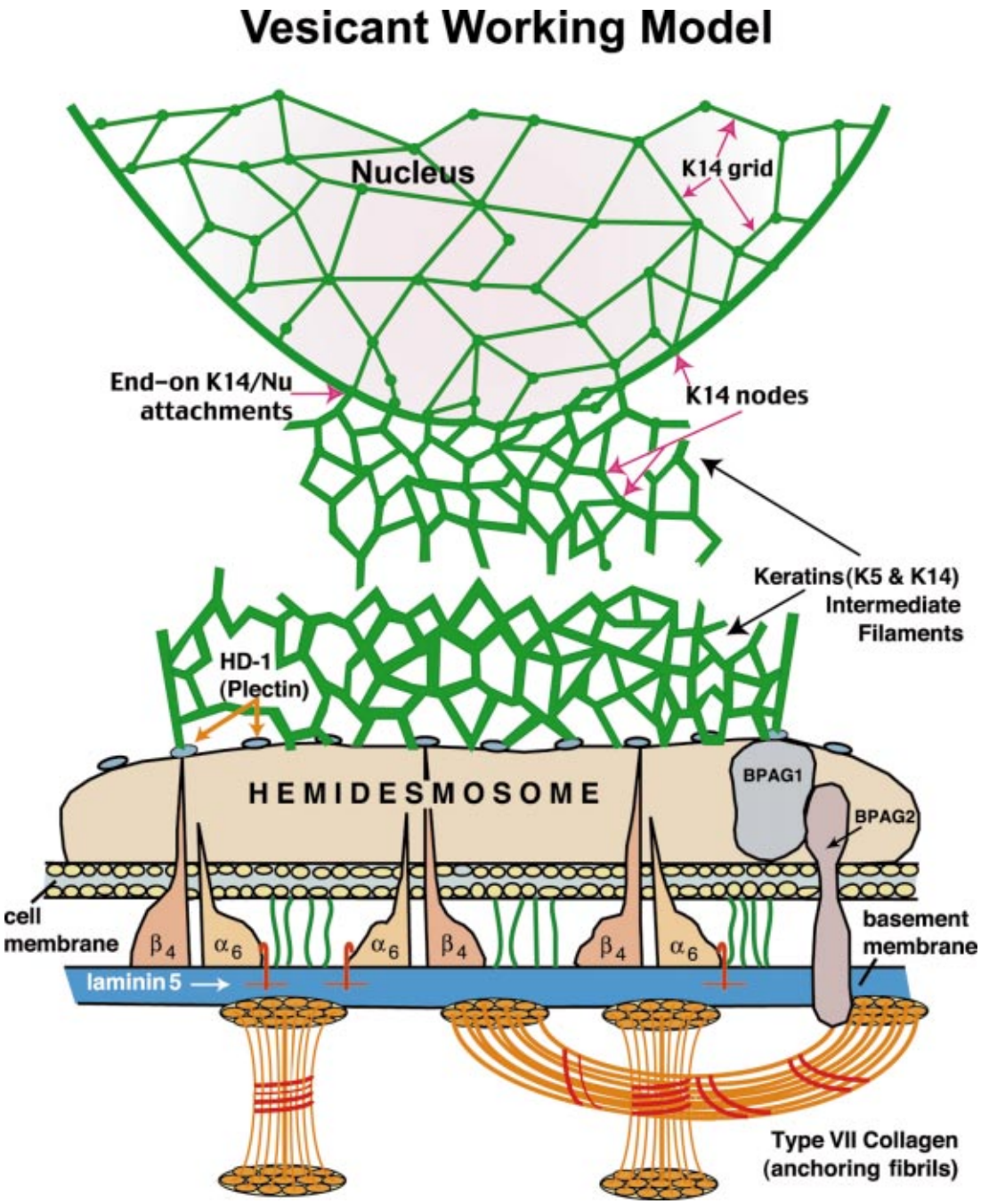

Fig. 11 Our vesicant working model has been developed from multiphoton imaging and from the structural and functional relationships of molecules shown to be disrupted by sulfur mustard. The target structures of interest include, but are not limited to, the heterodimeric keratin (K5/K14) intermediate filaments, the hemidesmosomes and proteins specific to the basal cell's adhesion complex, i.e., $\alpha_6\beta_4$ integrin receptors, laminin 5, plectin, bullous pemphigoid antigens G1 and G2 (BPAG1 and BPAG2). Progressive disruption of these structures by SM deprives basal cells of essential protein–protein interactions that link the uppermost surface of the nucleus to the extracellular matrix and provide a template for normal signal transduction. Knowing the detailed organization of target structures in this bidirectional signaling system, we can now use multiphoton microscopy with live cell and tissue preparations to augment development of effective treatment strategies.

separation, making it difficult to discriminate between cause and effect.

4 Discussion

4.1 *SM Effects on the Basal Cell Adhesion Complex*

Multiphoton microscopy and immunofluorescent imaging have given structural details that enhance our understanding of SM-induced pathogenic lesions. From postexposure images of human basal cells and epidermal tissues we now have compelling evidence that key molecules of the basal cell's adhesion complex are early targets of SM alkylation. These molecules include the intracellular, keratin 14 cytoskeleton, the transmembrane $\alpha_6\beta_4$ integrin receptors, and laminin 5, a ligand and bridging element to the basement membrane. Together with associated proteins, these well-integrated molecules link the basal cell's nucleus to the plasma membrane and provide a structural and functional continuum for basal cell adhesion and signal transduction.[29–32] It follows, therefore, that SM-induced disruptions in the structural integrity of adhesion complex molecules might also cause functional anomalies that interfere with maintenance and repair of epidermal–dermal attachments. In fact, the images did reveal losses in functional asymmetry, polarized mobility, and capacity to repair the adhesion complex, and ultimately the loss of cell viability (data not shown). All of these functions (motility, growth, repair, and anchorage-dependent viability) depend on signal transduction.[30,33,34] Therefore, our postexposure image profiles indicate that the ''window of opportunity'' for therapeutic treatment of SM lesions is limited by the early onset and progressive nature of their structural disruptions. Nevertheless, these same image profiles provide an important mechanistic and temporal basis for developing effective treatment strategies. To that end, we have assembled a working model (Fig. 11) for future studies on the treatment and resolution of SM effects on the adhesion complex and on the bidirectional signaling required for maintenance and repair of that complex. The model is a composite of information extrapolated from our multiphoton studies and from the literature.

4.2 *Effects of SM on Keratin 14*

Keratin 14 presented an elaborate response to SM that included (1) collapse of the K14 cytoskeleton; (2) loss of its open, airy, tentlike organization; (3) focal erosions; (4) dorsoventral stretching of K14 filaments collapsed over the nucleus; and (5) ventral displacement of the nucleus. Cytoskeletal collapse was progressive through the 6 h of postexposure study. That period of worsening conditions was consistent with the delayed onset of SM-induced blisters, which have a dose-dependent, clinical latent phase of 8 to 24 h.[4] In skin, however, SM-induced blisters do not form above the hemidesmosomes[4,15] as they do in EBS,[14] a family of blistering skin diseases linked to mutations that interfere with the assembly of K5/K14 filaments. It appears, therefore, that SM-induced collapse of the K14 cytoskeleton results from disruption of cytoskeletal organization and not from disruption of filament assembly. In complementary SM studies using sodium dodecyl sulphate–polyacrylamide gel electrophoresis (SDS-PAGE), Western blots, and densitometry, others have found a postexposure presence and accumulation of both low molecular weight K14 fragments (Mol, personal communication)[35] and high molecular weight K14 protein bands (Dillman et al.)[28] without any increase in K14 content.

4.3 *Effects of SM on $\alpha_6\beta_4$ Integrin and Laminin 5*

The strength and resilience of dermal–epidermal attachments have been clearly related to hemidesmosomes[25,36,37] and to their inherent $\alpha_6\beta_4$ integrin receptors.[38] They provide a nexus linking basal cell keratins (K5/K14) to laminin 5 and the basement membrane.[39–41] The distribution of integrin receptors on the epidermis (Fig. 8) and their effective role in providing anchoring sites for laminin 5 attachment (Fig. 9 and Fig. 10) are well served by the topographic complexity of the ventral epidermis. In fact, images presented in previous multiphoton studies[16] showed the extent to which $\alpha_6\beta_4$ integrins occupy the elaborate surface area provided by rete pegs and ridges. While the elaborate matrix of integrin receptors enhances the adhesive strength of epidermal–dermal junctions, it is increasingly clear that $\alpha_6\beta_4$ integrins and laminin 5 provide basal cells with much more than simple attachment sites. Together with other adhesion receptors and linker proteins, they convey positional information and mediate inside-out and outside-in communication between the basal cell and its extracellular environment.[42,43,33] As illustrated in Fig. 4, the structural continuum for bidirectional interaction in our system links the gridlike keratin 14 cytoskeleton to the dorsal surface of the nucleus and to a narrow rim of anchoring sites within the basolateral membrane margins (Fig. 1 and Fig. 2). Those membrane margins also contain a narrow band of $\alpha_6\beta_4$ integrins [Fig. 5(b)] that co-localize on (attach to) laminin 5 ligand deposits within 0.5 μm of the HEK attachment surface [Fig. 5(d)]. It is interesting to speculate how specific, well-directed nuclear responses to positional information from the extracellular environment and from the considerable matrix of $\alpha_6\beta_4$ receptors might be augmented by integration and signal averaging through the cytoskeletal-nuclear grid. According to the literature, the specificity of signal transduction involves specific ligand binding and both subunits of a given $\alpha\beta$ heterodimer.[30,33] That activation process requires conformational changes involving intracellular separation of the $\alpha\beta$ subunits[44,45] plus well-established integrin–cytoskeletal interactions.[46] We suggest that this highly involved and structure-dependent process would clearly be incapacitated by the progressive, disruptive effects of sulfur mustard. We also suggest that the structural lesions described in this study may potentiate vesication by disrupting signal transduction and the associated mechanisms required for maintenance and repair of the dermal–epidermal junction.

Acknowledgments

We gratefully acknowledge Stephanie Froberg and Theresa Tezak-Reid for their professional commitment, talent and assistance in preparing the illustrations for this manuscript. The opinions or assertions contained herein are the private views of the authors and are not to be construed as official or as reflecting the views of the Department of the Army or the Department of Defense.

References

1. W. Denk, D. Piston, and W. Webb, ''Two-photon molecular excitation in laser-scanning microscopy,'' Chapter 28 in *Handbook of Biological Confocal Microscopy*, J. Pawley, Ed., pp. 445–458, Plenum, New York (1995).
2. P. T. C. So, K. H. Kim, C. Buehler, B. R. Masters, L. Hsu, and C. Y. Dong, ''Basic principles of multiphoton excitation microscopy,'' Chapter 9 in *Methods in Cellular Imaging*, A. Periasamy, Ed., pp. 147–161, Oxford University Press, New York (2001).
3. V. P. Wallace, A. K. Dunn, M. O. Coleno, and B. Tromberg, ''Two-photon microscopy in highly scattering tissue,'' Chapter 11 in *Methods in Cellular Imaging*, A. Periasamy, Ed., pp. 180–199, Oxford University Press, New York (2001).
4. B. Papirmeister, A. Feister, S. Robinson, and R. Ford, *Medical Defense Against Mustard Gas: Toxic Mechanisms and Pharmacological Implications*, CRC Press, Boca Raton, FL (1991).
5. P. A. Coulombe, M. E. Hutton, R. Vassar, and E. Fuchs, ''A function for keratins and a common thread among different types of epidermolysis bullosa simplex diseases,'' *J. Cell Biol.* **115**, 1661–1674 (1991).
6. Y. Chan, I. Anton-Lamprecht, Q. C. Yu, A. Jäckel, B. Zabel, J. Ernst, and E. Fuchs, ''A human keratin 14 knockout: the absence of K14 leads to severe epidermolysis bullosa simplex and a function for an intermediate filament protein,'' *Genes Dev.* **8**, 2574–2587 (1994).
7. Y. Chan, J. Cheng, T. Gedde-Dahl, Jr., K. Niemi, and E. Fuchs, ''Genetic analysis of a severe case of Dowling-Meara epidermolysis bullosa simplex,'' *J. Invest. Dermatol.* **106**, 327–334 (1996).
8. E. Fuchs, ''Genetic disorders of keratins and their associated proteins,'' *J. Dermatol. Sci.* **13**, 181–192 (1996).
9. E. Fuchs, (Keith R. Porter Lecture, 1996), ''Of mice and men: genetic disorders of the cytoskeleton,'' *Mol. Biol. Cell* **8**, 189–203 (1997).
10. E. Fuchs, ''The cytoskeleton and disease: genetic disorders of intermediate filaments,'' *Annu. Rev. Genet.* **30**, 197–231 (1996).
11. R. J. Werrlein and J. S. Madren-Whalley, ''Effects of sulfur mustard on the basal cell adhesion complex,'' *J. Appl. Toxicol.* **20**, S115–S123 (2000).
12. R. J. Werrlein and J. S. Madren-Whalley, ''Imaging sulfur mustard lesions in human epidermal tissues and keratinocytes by confocal and multiphoton microscopy,'' in *Multiphoton Microscopy in the Biomedical Sciences II*, A. Periasamy and P. T. C. So, Eds., *Proc. SPIE* **4620**, 231–241 (2002).
13. J. Uttam, E. Hutton, P. A. Coulombe, I. Anton-Lamprecht, Q. C. Yu, T. Gedde-Dahle, Jr., J. D. Fine, and E. Fuchs, ''The genetic basis of epidermolysis bullosa simplex with mottled pigmentation,'' *Proc. Natl. Acad. Sci. U.S.A.* **93**, 9079–9084 (1996).
14. E. Fuchs and D. W. Cleveland, ''A structural scaffolding of intermediate filaments in health and disease,'' *Science* **279**, 514–519 (1998).
15. Z. Zhang, B. P. Peters, and N. A. Monteiro-Riviere, ''Assessment of sulfur mustard interaction with basement membrane components,'' *Cell Biol. Toxicol.* **11**, 89–101 (1995).
16. R. J. Werrlein and J. S. Madren-Whalley, ''Imaging sulfur mustard lesions in basal cells and human epidermal tissues by confocal and multiphoton laser-scanning microscopy,'' Chapter 27 in *Alternative Toxicological Methods*, H. S. Salem and S. Katz, Eds., pp. 303–312, CRC Press, Boca Raton, FL (2003).
17. L. Spinardi, Y. L. Ren, R. Sanders, and F. G. Giancotti, ''The β_4 subunit cytoplasmic domain mediates the interaction of the $\alpha_6\beta_4$ integrin with the cytoskeleton of the hemidesmosomes,'' *Mol. Biol. Cell* **4**, 871–884 (1993).
18. R. Foisner, F. E. Leichfried, H. Hermann, J. V. Small, D. Lawson, and G. Wiche, ''Cytoskeleton associated plectin: *in situ* localization, *in vitro* reconstitution, and binding to immobilized intermediate filament proteins,'' *J. Cell Biol.* **106**, 723–733 (1988).
19. R. Foisner, W. Bohn, K. Mannweiler, and G. Wiche, ''Distribution and ultrastructure of plectin arrays in subclones of rat glioma 6 cells differing in intermediate filament protein (vimentin) expression,'' *J. Struct. Biol.* **115**, 304–317 (1995).
20. G. Wiche, R. Krepler, U. Artlieb, R. Pytela, and W. Aberer, ''Identification of plectin in different human cell types and immunolocalization at epithelial basal cell surface membranes,'' *Exp. Cell Res.* **155**, 43–49 (1984).
21. G. Wiche, D. Gromov, A. Donovan, M. J. Castañon, and E. Fuchs, ''Expression of plectin mutant cDNA in cultured cells indicates a role of COOH-terminal domain in intermediate filament association,'' *J. Cell Biol.* **121**, 607–619 (1993).
22. S. B. Hopkinson, K. Findlay, G. W. deHart, and J. C. R. Jones, ''Interaction of BP180 (type XVII collagen) and α_6 integrin is necessary for stabilization of hemidesmosome structure,'' *J. Invest. Dermatol.* **111**, 1015–1022 (1998).
23. L. Guo, L. Degenstein, J. Dowling, Q. C. Yu, R. Wollmann, B. Perman, and E. Fuchs, ''Gene targeting of BPAG1: cell migration in stratified epithelia and neurologic degeneration,'' *Cell* **81**, 233–243 (1995).
24. S. E. Baker, S. B. Hopkinson, M. Fitchmun, G. L. Andreason, F. Frasier, G. Plopper, V. Quaranta, and J. C. R. Jones, ''Laminin 5 and hemidesmosomes: Role of the α_3-chain subunit in hemidesmosome stability and assembly,'' *J. Cell. Sci.* **109**, 2509–2520 (1996).
25. J. C. Jones, S. B. Hopkinson, and L. E. Goldfinger, ''Structure and assembly of hemidesmosomes,'' *BioEssays* **21**(6), 488–494 (1998).
26. L. Pulkkinen and J. Uitto, ''Hemidesmosomal variants of epidermolysis bullosa,'' *Exp. Dermatol.* **7**, 46–64 (1998).
27. R. Werrlein, T. Hamilton, and J. S. Madren-Whalley, ''Development of human keratinocyte colonies for confocal microscopy and for study of calcium effects on growth differentiation and sulfur mustard lesions,'' Chapter 14 in *Toxicity Assessment Alternatives: Methods, Issues, Opportunities*, H. Salem and S. Katz, Eds., pp. 165–174, Humana Press, Totowa, NJ (1999).
28. J. F. Dillman III, K. L. McGary, and J. S. Schlager, ''Sulfur mustard-induced high molecular weight aggregates of keratins K5 and K14 in human epidermal keratinocytes,'' (submitted).
29. C. Jamora and E. Fuchs, ''Intercellular adhesion signaling and the cytoskeleton,'' *Nat. Cell Biol.* **4**(4), E101–E108 (2002).
30. R. O. Hynes, ''Integrins: bi-directional, allosteric signaling machines,'' *Cell* **110**, 673–687 (2002).
31. G. Delwel and A. Sonnenberg, ''Laminin isoforms and their integrin receptors,'' Chapter 2 in *Adhesion Receptors as Therapeutic Targets*, M. A. Horton, Ed., pp. 9–36, CRC Press, Boca Raton, FL (1996).
32. F. Mainiero, A. Pepe, K. K. Wary, L. Spinardi, M. Mohammadi, J. Schlessinger, and F. G. Giancotti, ''Signal transduction by the $\alpha_6\beta_4$ integrin: distinct β_4 subunit sites mediate recruitment of Shc/Grb2 and association with the cytoskeleton of hemidesmosomes,'' *EMBO J.* **14**, 4470–4481 (1995).
33. T. Pawson and P. Nash, ''Protein-protein interactions define specificity in signal transduction,'' *Genes Dev.* **14**, 1027–1047 (2000).
34. M. A. Schwartz and R. K. Assoian, ''Integrins and cell proliferation: regulation of cyclin-dependent kinases via cytoplasmic signaling pathways,'' *J. Cell. Sci.* **114**, 2553–2560 (2001).
35. M. Mol, ''Sulfur mustard induces low molecular weight fragments of keratin 14 in human epidermal keratinocytes,'' (in preparation).
36. L. Borradori and A. Sonnenberg, ''Hemidesmosomes: Roles in adhesion, signaling and human diseases,'' *Curr. Opin. Cell Biol.* **8**, 647–656 (1996).
37. M. G. Nievers, R. Q. J. Schaapveld, and A. Sonnenberg, ''Biology and function of hemidesmosomes,'' *Matrix Biol.* **18**, 5–17 (1999).
38. M. A. Stepp, S. Spurr-Michaud, A. Tisdale, J. Elwell, and I. K. Gipson, ''$\alpha_6\beta_4$ Integrin heterodimer is a component of hemidesmosomes,'' *Proc. Natl. Acad. Sci. U.S.A.* **87**, 8970–8974 (1990).
39. J. C. R. Jones, J. Asmuth, S. E. Baker, M. Langhofer, S. I. Roth, and S. B. Hopkinson, ''Hemidesmosomes: Extracellular matrix/intermediate filament connectors,'' *Exp. Cell Res.* **213**, 1–11 (1994).
40. R. E. Burgeson and A. M. Christiano, ''The dermal-epidermal junction,'' *Curr. Opin. Cell Biol.* **9**, 651–658 (1997).
41. J. Dowling, Q. C. Yu, and E. Fuchs, ''β_4 Integrin is required for hemidesmosomal formation, cell adhesion and cell survival,'' *J. Cell Biol.* **134**, 559–572 (1996).
42. C. Rosales, V. O'Brien, L. Kornberg, and R. Juliano, ''Signal transduction by cell adhesion receptors,'' *Biochem. Biophys. Acta* **1242**, 77–98 (1995).
43. L. Borradori and A. Sonnenberg, ''Structure and function of hemidesmosomes: more than simple adhesion complexes,'' *J. Invest. Dermatol.* **112**, 411–418 (1999).
44. J. Takagi, H. P. Erickson, and T. A. Springer, ''C-terminal opening mimics 'inside-out' activation of integrin alpha 5 beta 1,'' *Nat. Struct. Biol.* **8**, 412–416 (2001).
45. J. Takagi, B. M. Petre, T. Walz, and T. A. Springer, ''Global conformational rearrangements in integrin extracellular domains in outside-in and inside-out signaling,'' *Cell* **110**, 599–611 (2002).
46. S. M. Schoenwaelder and K. Burridge, ''Bidirectional signaling between the cytoskeleton and integrins,'' *Curr. Opin. Cell Biol.* **11**, 274–286 (1999).